Analysis of Nonsquare Artificial Dielectric Layers and Application to the Design of Anisotropic Slabs

van Schelven, Ralph M.; Cavallo, Daniele

Important note
To cite this publication, please use the final published version (if applicable).
Please check the document version above.

Analysis of Nonsquare Artificial Dielectric Layers and Application to the Design of Anisotropic Slabs

Ralph M. van Schelven 🄳, *Student Member, IEEE*, and Daniele Cavallo 🄳, *Senior Member, IEEE*

Abstract—**We present a general analysis to describe nonsquare artificial dielectric layers (ADLs). Closed-form expressions for the equivalent layer impedance are given for generic plane-wave incidence, assuming that the ADLs have different geometrical parameters in the x- and y-directions. The analytical expressions account for the interaction between the layers due to higher order Floquet modes, thus remain valid for arbitrarily small electrical distance between layers. Such nonsquare geometries allow the design of artificial anisotropic slabs with azimuth-dependent effective refractive index. As an example for an application, the equivalent model is used to design the superstrate of a double-slot antenna, with independent pattern shaping in the two main planes.**

Index Terms—**Artificial dielectrics, equivalent circuit, pattern shaping, spectral domain methods.**

I. INTRODUCTION

ARTIFICIAL dielectric layers (ADLs) are stacks of planar layers, each composed of periodic subwavelength metal structures, engineered to realize a material with a desired effective refractive index [1], [2]. The equivalent electromagnetic parameters of the ADLs can be controlled by varying the period and the shape of the metallic patches, and the interlayer distance [3]. Due to the planarity of the patches, the ADL slabs are anisotropic, and thus, their effective refractive index changes as a function of the polarization and of the incidence angle of an impinging plane wave. This property was recently exploited to improve the front-to-back ratio and the bandwidth of planar antennas without exciting the surface waves [4], or equivalently to enlarge the bandwidth and the scan range of broadband arrays, with no scan blindness [5].

For the electromagnetic modeling of ADLs, a number of numerical solutions have been proposed for the efficient analysis of generic multilayer metasurfaces, for example [6]–[8]. However, these methods assume that the current profile on the unit cell is obtained with a full-wave simulation, for example by means of a spectral method of moments or another numerical method.

More recently, analytical formulas to describe ADLs based on subwavelength square patches were presented in [9] for aligned layers [see Fig. 1(a)] and generalized in [10] to include a shift between the even and odd layers [see Fig. 1(b)]
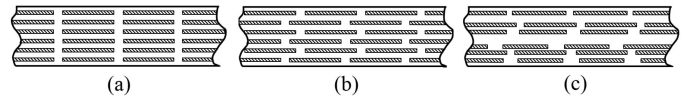
Fig. 1.   2-D side view for artificial dielectric slabs with (a) aligned, (b) shifted, and (c) nonperiodic layers along z.

and in [11] for nonperiodic layers along z [see Fig. 1(c)]. All the mentioned works provide a transmission line model to represent the propagation of a generic plane wave within the ADLs. In such equivalent circuit, each layer is represented as an equivalent shunt impedance, which can be expressed in the closed form as a function of the geometrical parameters of the ADLs. Alternative analytical expressions for a single layer of square patches were given in [12]–[14]. When compared to these alternative expressions, the main advantage of the formulation used here is that it is easy to generalize into multiple layers. The equivalent impedance of each layer include the reactive coupling between layers due to higher order Floquet modes; thus, it is still accurate for a very small electrical distance between the layers, which is common in ADL designs.

A limitation of the previously published analyses of ADLs is the assumption of square patches and unit cells. Because of the square shape, many terms during the derivation of the analytical expressions simplify, resulting in the decoupling of the transverse electric (TE) and transverse magnetic (TM) modes in the equivalent transmission line model. In this letter, nonsquare geometries are investigated and more general closed-form expressions are derived for the first time to account for rectangular unit cells. The different geometrical parameters along x and y allow for an extra degree of freedom in the design of ADL slabs. We show, for example, that one can design an antenna superstrate with the intent to shape the radiation pattern independently in the E- and H-planes. Another possible application of the given anisotropic superstrate would be the design of linear-to-linear or linear-to-circular polarization converters, where the independent control of the refractive index for TE- and TM-polarized incident plane waves can be used for achieving the desired phase shift between the TE and TM components.

II. CLOSED-FORM ANALYSIS OF NONSQUARE ADLs

A. Admittance Matrix of a Single Layer

The theory of ADLs developed in earlier works [9]–[11] always considered square patches arranged in a square
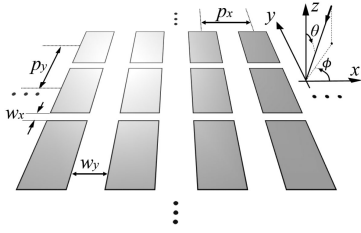
Fig. 2. Single layer of rectangular patches, where both the period and the width of the gaps between the patches can be different along x and y.
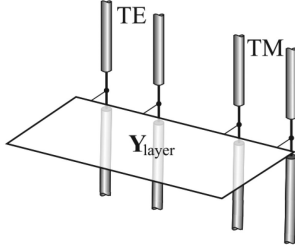

Fig. 3. Equivalent transmission line model for a plane wave incident on a layer of periodic rectangular patches. The layer is represented as a 2-port admittance matrix $\mathbf{Y}_{\text{layer}}$.
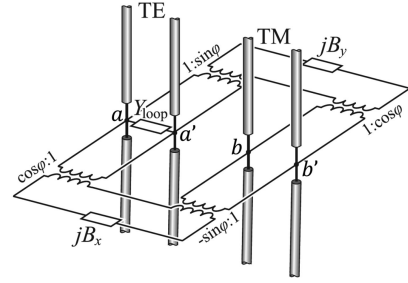

Fig. 4. Explicit representation of the equivalent circuit representing the layer.
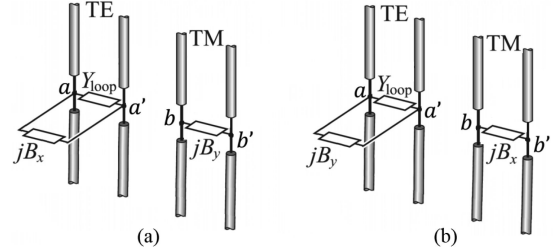
Fig. 5. Simplified Equivalent circuit for (a) $\phi = 0°$ and (b) $\phi = 90°$.

periodic lattice. This assumption greatly simplifies the analysis, because for square patches, small compared to the wavelength, the TE and TM modes of the plane wave are decoupled, and the equivalent reactance of the layer is a single shunt load for each mode, independent of the Azimuth angle of incidence (ϕ). When considering rectangular layers, as shown in Fig. 2, these simplifications cannot be made, and in general, the layer reactance is represented as a two-port admittance matrix connecting the plane-wave equivalent TE and TM transmission lines, as depicted in Fig. 3. The characteristic impedances of the TE and TM transmission lines are $Z^{\text{TE}} = \zeta / \cos\theta$ and $Z^{\text{TM}} = \zeta \cos\theta$, respectively, where ζ is the intrinsic impedance of the medium embedding the layer, and θ is the elevation angle of the incident plane wave.

By applying the same spectral domain method as in [10], the admittance matrix of the nonsquare layer is found as

$$\mathbf{Y}_{\text{layer}}$$
$$= \begin{bmatrix} jB_y\sin^2\phi + jB_x\cos^2\phi + Y_{\text{loop}} & j\sin\phi\cos\phi(B_y - B_x) \\ j\sin\phi\cos\phi(B_y - B_x) & jB_x\sin^2\phi + jB_y\cos^2\phi \end{bmatrix} \tag{1}$$

where Y_{loop} is a term related to the TE incidence, associated with current loops over the patches, given by

$$Y_{\text{loop}} = \sin^2\theta \left(\frac{j}{B_x} + \frac{j}{B_y} \right)^{-1}. \tag{2}$$

The terms B_x and B_y are the susceptances of the x- and y-oriented slots, respectively, expressed as Floquet sums

$$B_x = \frac{\omega\varepsilon_0\varepsilon_{\text{av}}p_y}{\pi} \sum_{m\neq 0} S_m\left(\frac{w_x}{p_y} \right) \tag{3}$$

$$B_y = \frac{\omega\varepsilon_0\varepsilon_{\text{av}}p_x}{\pi} \sum_{m\neq 0} S_m\left(\frac{w_y}{p_x} \right) \tag{4}$$

where $S_m(x) = |\text{sinc}(\pi m x)|^2/|m|$, ε_0 is the vacuum permittivity, and ε_{av} is the average relative permittivity of the media above and below the layer.

It can be seen from (1) that the TE and the TM transmission lines are not decoupled as the matrix is not diagonal. The expression in (1) can be represented as the explicit equivalent circuit in Fig. 4. The dependence of the Azimuth angle is included in impedance transformers connected to the susceptances of the x- and y-oriented slots. For square ADL (i.e., $B_x = B_y$), it can be seen that the matrix in (1) simplifies to a diagonal matrix, as expected, resulting in decoupled TE and TM transmission lines. This effect can be also observed from the circuit in Fig. 4. Under the condition $B_x = B_y$, for a purely TE incident wave, the incident voltage splits in the two branches of the circuit at the terminals aa' and forms two equal and opposite contributions when reaching the terminals bb'. This is due to the different signs of the transformers $\pm \sin\phi$ in the two branches. Since the total voltage is 0 at bb', it is equivalent to a short circuit, and thus, no coupling occurs between TE and TM modes. Similarly, a purely TM incident wave would generate an equivalent short circuit at the terminal aa' and remains decoupled from the TE transmission line. Therefore, the given formulation also holds for square ADL.

Even for the nonsquare geometries, the layer matrix can be diagonalized on the two crystal angles, as in [15] and [16]. For the geometry under investigation, the two angles are $\phi = 0°$ and $\phi = 90°$ and do not depend on frequency, because of the symmetric nature of the geometry [16]. For these two angles, the equivalent circuit simplifies, as shown in Fig. 5.

B. Analysis of Multiple Layers

The generalization to multiple layers can be obtained, as in [11]. With reference to Fig. 6, the susceptance of the nth layer depends on the geometrical parameters of the layer
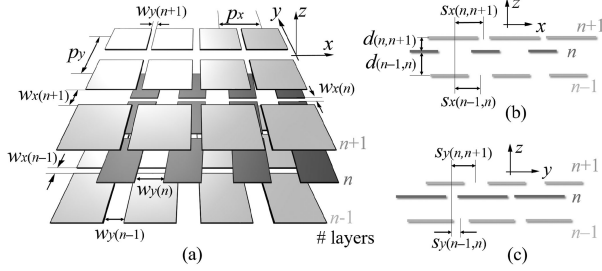
Fig. 6. Geometrical parameters of the multilayer of nonsquare ADLs. (a) 3-D view. (b) (xz)-plane side view. (c) (yz)-plane side view.

itself and the parameters of the layers above and below. For example, the susceptance B_x of the nth layer becomes

$$B_{x(n)} = \frac{\omega \varepsilon_0 \varepsilon_{\mathrm{av}} p_y}{\pi} \sum_{m \neq 0}$$

$$\left\{ S_m \left(\frac{w_{x(n)}}{p_y} \right) \left[f_m \left(\frac{d_{(n-1,n)}}{p_y} \right) + f_m \left(\frac{d_{(n,n+1)}}{p_y} \right) \right] \right.$$

$$+ S_m \left(\frac{w_{x(n-1)}}{p_y} \right) g_m \left(\frac{d_{(n-1,n)}}{p_y}, \frac{s_{y(n-1,n)}}{p_y} \right)$$

$$\left. + S_m \left(\frac{w_{x(n+1)}}{p_y} \right) g_m \left(\frac{d_{(n,n+1)}}{p_y}, \frac{s_{y(n,n+1)}}{p_y} \right) \right\}$$

(5)

where $f_m(x) = -0.5j \cot(-2j\pi|m|x)$ and $g_m(x,y) = 0.5j \csc(-2j\pi|m|x) \exp(2i\pi y)$, and the suceptance B_y has the same expression but substituting $p_y \to p_x$, $w_x \to w_y$, and $s_y \to s_x$.

Slightly different expressions can be used for the first and last layers

$$B_{x(1)} = \frac{\omega \varepsilon_0 \varepsilon_{\mathrm{av}} p_y}{\pi} \sum_{m \neq 0} \left\{ S_m \left(\frac{w_{x(1)}}{p_y} \right) \left[\frac{1}{2} + f_m \left(\frac{d_{(1,2)}}{p_y} \right) \right] \right.$$

$$\left. + S_m \left(\frac{w_{x(2)}}{p_y} \right) g_m \left(\frac{d_{(1,2)}}{p_y}, \frac{s_{y(1,2)}}{p_y} \right) \right\}$$

(6)

$$B_{x(N)} = \frac{\omega \varepsilon_0 \varepsilon_{\mathrm{av}} p_y}{\pi} \sum_{m \neq 0} \left\{ S_m \left(\frac{w_{x(N)}}{p_y} \right) \left[\frac{1}{2} + f_m \left(\frac{d_{(N-1,N)}}{p_y} \right) \right] \right.$$

$$\left. + S_m \left(\frac{w_{x(N-1)}}{p_y} \right) g_m \left(\frac{d_{(N-1,N)}}{p_y}, \frac{s_{y(N-1,N)}}{p_y} \right) \right\}.$$

(7)

To find the S-parameters of the total multilayer structure, one can cascade the four-port networks of each individual layer, as shown in Fig. 7. The transmission and reflection coefficients for the entire stack can be obtained with the method for connecting N-port networks, as described in [17].

C. Validity of the Model

To assess the validity of the model, a comparison with the CST full-wave simulations is shown for different geometry examples. Two cases are considered, both with the metal
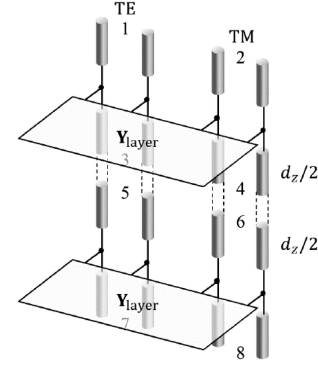

Fig. 7. Total transmission-line model split into separate four-ports for each layer.

TABLE I
GEOMETRICAL PARAMETERS FOR THE THREE CONSIDERED STRUCTURES; λ IS THE WAVELENGTH AT THE CALCULATION FREQUENCY f_0

	Case 1	Case 2
N	5	5
p_x	0.15λ	0.2λ
p_y	0.2λ	0.15λ
$d_{(n,n+1)}$ for $n \in [1, N-1]$	0.012λ	0.012λ
$w_{x(n)}$ for $n \in [1, N]$	0.01λ	0.04λ
$w_{y(n)}$ for $n \in [1, N]$	0.02λ	0.01λ
$s_{x(n,n+1)}$ for $n \in [1, N-1]$	0	$0.5p_x$
$s_{y(n,n+1)}$ for $n \in [1, N-1]$	0	0
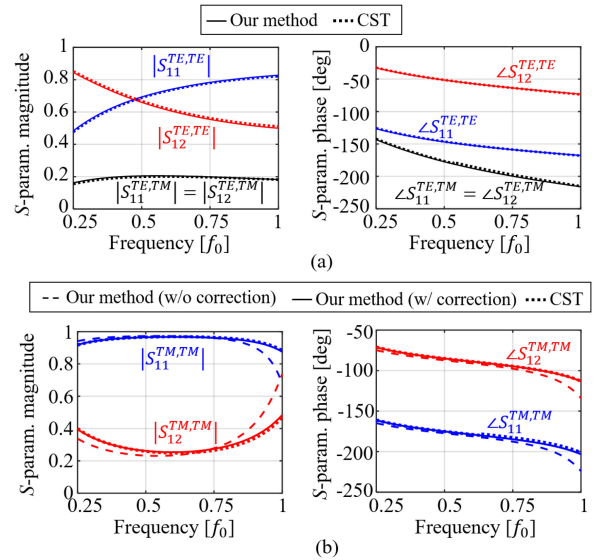
Fig. 8. Scattering parameters of a plane wave. (a) Incident from $\theta = 45°$ and $\phi = 45°$ on ADLs with parameters in Table 1 (Case 1). (b) Incident from $\theta = 0°$ and $\phi = 0°$ on ADLs with parameters in Table 1 (Case 2).

patches located in the free space, with the geometrical parameters specified in Table I.

For Case 1, we consider a TE plane-wave incident from $\theta = 45°$ and $\phi = 45°$. The resulting S-parameters, amplitude, and phase are shown in Fig. 8(a). A very good agreement can be seen between the equivalent circuit given here and CST. For Case 2, a TM plane-wave incident from $\theta = 0°$ and $\phi = 0°$ is considered. The geometry refers to a large ratio

Fig. 9. Electric field distribution between the patches of an ADL. (a) Assumed distribution. (b) Real distribution when w_x and w_y are comparable. (c) Real distribution for large ratio w_y/w_x. (d) Equivalent connected dipole gap.
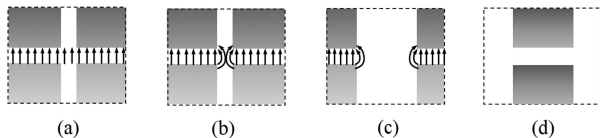
between the two slot widths along x and y. A worse agreement is observed in this example, especially at the higher frequency, as shown in Fig. 8(b). The discrepancy can be attributed to the assumption on the electric field distribution in the slots. The given expressions for the susceptance in (5)–(7) assume that the electric field distribution is uniform on a slot [see Fig. 9(a)], as if there was no crossing slot. The real distribution has some fringing effect at the junction, as depicted in Fig. 9(b), which do not significantly change the distribution as long as the two slot widths are comparable. However, for large ratios w_y/w_x, the electric field is not distributed over the entire unit cell [see Fig. 9(c)], resulting in a lower capacitance.

This effect can be corrected by comparing the susceptance B_x of a single layer in (3) with the gap susceptance of a connected dipole array B_{CDA} [see Fig. 9(d)], which was given in [18]. The correction factor B_{CDA}/B_x can be used to multiply the layer susceptances (5)–(7), resulting in a better comparison with CST, as shown in Fig. 8(b). It is important to note that the proposed correction technique can be applied as long as the inductive effect of the patches is small compared to the gap capacitance. When the patches become narrow strips, the formulation in terms of slot capacitance does no longer effectively represent the layer, because the inductance of the strip is neglected in the interlayer interaction.

III. APPLICATION EXAMPLE

As an example for an application of the nonsquare ADLs, we consider a double-slot antenna in the presence of an artificial dielectric superstrate. The ADLs can serve as a partially reflective surface that allows the propagation of leaky waves between the ADLs and slot plane, which can be used to shape the radiation pattern [19]–[23].

The design of the ADLs can be obtained from the desired values of the x- and y-components of the effective permittivity tensor (ε_x and ε_y) by applying the homogenization procedure described in [24]. The S-parameters of an incident plane wave for normal and oblique incidence, found from the circuit in Fig. 7, can be used to evaluate the effective permittivity and permeability tensors. In the design procedure, increasing the metal density (i.e., reducing the interlayer distance, the gap between patches, or the shift) allows increasing the effective refractive index.

Fig. 10(a) shows the geometry under consideration. The geometrical parameters are chosen as $l = 0.85\,\lambda$, $w = 0.05\,\lambda$, and $d_{\mathrm{sep}} = 0.5\,\lambda$, where λ is the free-space wavelength at the calculation frequency. Fig. 10(b) shows the normalized radiation pattern in the E- and H-plane of the double-slot antenna without the ADL. A four-layer square ADL with
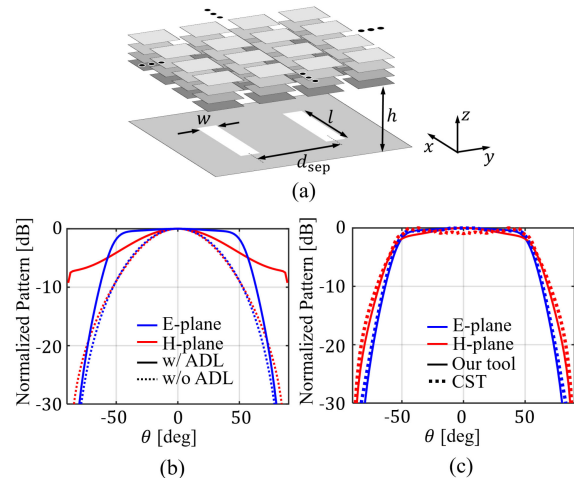

Fig. 10. (a) Double-slot antenna in the presence of an ADL superstrate. Normalized E- and H-plane radiation patterns (b) with and without square ADLs and (c) with nonsquare ADL. For the nonsquare ADL superstrate, a comparison with CST is shown.

$p_x = p_y = 0.15\,\lambda$, $w_x = w_y = 0.02\,\lambda$, $d = 0.015\,\lambda$, and $s_x = s_y = 0$ for all layers is located at a distance $h = 012\lambda$ from the slots. The ADL parameters are selected to shape the radiation in the E-plane as a flat-top pattern with larger beamwidth. It can be seen in Fig. 10(b) that the square ADL supestrate results in a very asymmetric pattern in the two main planes. However, by changing the ADL to have a nonsquare unit cell with $p_x = 0.25\,\lambda$ and $s_x = p_x/2$, the H-plane pattern can be shaped to have a similar flat-top characteristic as in the E-plane, while the E-plane pattern remains unaltered, as shown in Fig. 10(c). In the figure, the patterns are calculated by combining the equivalent circuit described here with a plane-wave expansion of the double-slot near field, as described in [9]. A comparison with CST is also reported.

IV. CONCLUSION

We presented analytical formulas for the analysis of non-periodic nonsquare ADLs with different geometrical parameters in x- and y-directions. Closed-form expressions for the equivalent layer impedance for the generic plane-wave incidence were derived, both for single and multiple layers. Based on the expression, an equivalent circuit of the layer was proposed, which explicitly includes the coupling between TE and TM components of the incident wave and the dependence on the incident angles. The accuracy of the method was discussed, and a correction term based on the gap capacitance of a connected dipole array was introduced to extend the validity of the method to larger aspect ratios of the patches.

A possible application of nonsquare ADLs was investigated, which consists of a double-slot antenna with an ADL superstrate to enlarge the beamwidth and to provide a flat-top radiation pattern. It was shown that the additional degree of freedom provided by the nonsquare ADLs could be used to render the symmetrical patterns in the E- and H-plane.

REFERENCES

[1] W. E. Kock, "Metallic delay lenses," *Bell Syst. Tech. J.*, vol. 27, no. 1, pp. 58–82, Jan. 1948.

[2] S. S. D. Jones and J. Brown, "Metallic delay lenses," *Nature*, vol. 163, no. 4139, pp. 324–325, Feb. 1949.

[3] R. E. Collin, *Field Theory of Guided Waves*, 2nd ed. New York, NY, USA: IEEE Press, 1990.

[4] D. Cavallo, W. H. Syed, and A. Neto, "Artificial dielectric enabled antennas for high frequency radiation from integrated circuits," in *Proc. 11th Eur. Conf. Antennas Propag.*, 2017, pp. 1626–1628.

[5] D. Cavallo, W. H. Syed, and A. Neto, "Connected-slot array with artificial dielectrics: A 6 to 15 GHz dual-pol wide-scan prototype," *IEEE Trans. Antennas Propag.*, vol. 66, no. 6, pp. 3201–3206, Jun. 2018.

[6] E. Martini, G. M. Sardi, and S. Maci, "Homogenization processes and retrieval of equivalent constitutive parameters for multisurface-metamaterials," *IEEE Trans. Antennas Propag.*, vol. 62, no. 4, pp. 2081–2092, Apr. 2014.

[7] S. Barzegar-Parizi and B. Rejaei, "Calculation of effective parameters of high permittivity integrated artificial dielectrics," *Microw., Antennas Propag.*, vol. 9, no. 12, pp. 1287–1296, Sep. 2015.

[8] F. Mesa, R. Rodríguez-Berral, M. García-Vigueras, F. Medina, and J. R. Mosig, "Simplified modal expansion to analyze frequency-selective surfaces: An equivalent circuit approach," *IEEE Trans. Antennas Propag.*, vol. 64, no. 3, pp. 1106–1111, Mar. 2016.

[9] D. Cavallo, W. H. Syed, and A. Neto, "Closed-form analysis of artificial dielectric layers − Part II: Extension to multiple layers and arbitrary illumination," *IEEE Trans. Antennas Propag.*, vol. 62, no. 12, pp. 6265–6273, Dec. 2014.

[10] D. Cavallo and C. Felita, "Analytical formulas for artificial dielectrics with nonaligned layers," *IEEE Trans. Antennas Propag.*, vol. 65, no. 10, pp. 5303–5311, Oct. 2017.

[11] D. Cavallo and R. M. van Schelven, "Closed-form analysis of artificial dielectric layers with non-periodic characteristics," in *Proc. 13th Eur. Conf. Antennas Propag.*, 2019, pp. 1–5.

[12] J. R. Wait, "Theories of scattering from wire-grid and mesh structures," *Electromagn. Scattering*, P. L. E. Uslenghi, Ed. New York, NY, USA: Academic, 1978, pp. 253–287.

[13] R. C. Compton and D. B. Rutledge, "Approximation techniques for planar periodic structures," *IEEE Trans. Microw. Theory Techn.*, vol. 33, no. 10, pp. 1083–1088, Oct. 1985.

[14] O. Luukkonen *et al.*, "Simple and accurate analytical model of planar grids and high-impedance surfaces comprising metal strips or patches," *IEEE Trans. Antennas Propag.*, vol. 56, no. 6, pp. 1624–1632, Jun. 2008.

[15] C. Pfeiffer and A. Grbic, "Bianisotropic metasurfaces for optimal polarization control: Analysis and synthesis," *Phys. Rev. Appl.*, vol. 2, no. 4, Oct. 2014, Art. no. 044011.

[16] M. Borgese and F. Costa, "A simple equivalent circuit approach for anisotropic frequency-selective surfaces and metasurfaces," *IEEE Trans. Antennas Propag.*, vol. 68, no. 10, pp. 7088–7098, Oct. 2020.

[17] E. Salerno, "Appunti di microonde," (in Italian). Accessed: May 12, 2021. [Online]. Available: http://www1.isti.cnr.it/ salerno/Microonde/ Microonde_08062010.pdf

[18] D. Cavallo, A. Neto, and G. Gerini, "Green's function based equivalent circuits for connected arrays in transmission and in reception," *IEEE Trans. Antennas Propag.*, vol. 59, no. 5, pp. 1535–1545, May 2011.

[19] G. V. Trentini, "Partially reflecting sheet arrays," *IRE Trans. Antennas Propag.*, vol. AP-4, no. 4, pp. 666–671, Oct. 1956.

[20] R. Gardelli, M. Albani, and F. Capolino, "Array thinning by using antennas in a Fabry–Perot cavity for gain enhancement," *IEEE Trans. Antennas Propag.*, vol. 54, no. 7, pp 1979–1990, Jul. 2006.

[21] A. Neto, N. Llombart, G. Gerini, M. Bonnedal, and P. de Maagt, "EBG enhanced feeds for the improvement of the aperture efficiency of reflector antennas," *IEEE Trans. Antennas Propag.*, vol. 55, no. 8, pp. 2185–2193, Aug. 2007.

[22] A. Neto, M. Ettorre, G. Gerini, and P. de Maagt, "Leaky wave enhanced feeds for multibeam reflectors to be used for telecom satellite based links," *IEEE Trans. Antennas Propag.*, vol. 60, no. 1, pp. 110–120, Jan. 2012.

[23] D. Blanco, N. Llombart, and E. Rajo-Iglesias, "On the use of leaky wave phased arrays for the reduction of the grating lobe level," *IEEE Trans. Antennas Propag.*, vol. 62, no. 4, pp. 1789–1795, Apr. 2014.

[24] D. Cohen and R. Shavit, "Bi-anisotropic metamaterials effective constitutive parameters extraction using oblique incidence S-parameters method," *IEEE Trans. Antennas Propag.*, vol. 63, no. 5, pp. 2071–2078, May 2015.